

Title: Antiskyrmionic ferroelectric medium

Authors: Mauro A. P. Gonçalves¹, Marek Paściak¹, Jiří Hlinka^{1*}

Affiliations:

¹Institute of Physics, Czech Academy of Sciences; Prague, 182 21, Czech Republic.

*Corresponding author. Email: hlinka@fzu.cz

Abstract:

Magnetization knots, known as ferromagnetic skyrmions, are string-like nanoobjects with a vortex-like spin texture. By now they have been found in many chiral ferromagnets. At the same time, there is only one material known to form geometrically equivalent vortices of ferroelectric polarization, the crystal of lead titanate. Our density functional theory based atomistic simulations now reveal that in a related material barium titanate, intrinsic string-like vortexes of another type are stable instead of skyrmions - ferroelectric antiskyrmions. They remind ring windings of decorative knots, have just 2-3 nm in diameter, possess a hexagonal section and an exotic topological charge of minus two. These findings suggest that ferroelectrics might in principle serve as memory media operating with nanoscale topological line defects and that they could be antiskyrmion forming media rather than skyrmion media.

One-Sentence Summary:

Ultrasmall nanodomains in barium titanate spontaneously develop a negative topological charge.

Main Text:

Discovery of the topologically stable nanoscale swirling defects of magnetization textures in chiral ferromagnets (1, 2), termed as magnetic skyrmions, has opened amazing perspectives for information storage technology (3) as well as a vast arena for studies of intriguing new physics phenomena (4, 5) like the topological Hall effect (6) and the skyrmion Hall effect (7–9). It is now well understood that topological defects like skyrmions, merons, bimerons, hedgehogs (10), hopfions (11), skyrmionia (12, 13) and antiskyrmions can be stabilized in many other, sometimes even achiral or centrosymmetric, magnets and antiferromagnets (14, 15).

Geometrically analogous nanoscale swirling defects of electric polarization textures have been also observed in nonmagnetic ferroelectric materials (16). These ferroelectric skyrmions have been attracting attention due to their truly nanoscale size (16–18) and intriguing physical properties such as negative capacitance (19) or emergent chirality (20–24). Ferroelectric skyrmions have been successfully induced by tailoring the geometry of suitable paraelectric-ferroelectric nanocomposites (16), but formation of the skyrmions was predicted to occur even in the bulk ferroelectric lead titanate, PbTiO_3 .

Such an intrinsic columnar nanodomain, studied in the reference (17), is sketched in Fig. 1a. The nanodomain, defined by the polarization parallel to z direction, is surrounded by a matrix of the opposite polarization. It was found that an in-plane polarization develops at the domain wall, forming a closed loop. The resulting polarization arrangement corresponds to a Bloch-like skyrmion.

Both magnetic and ferroelectric skyrmions are string-like defects in a vector order parameter field. The non-trivial topology of the skyrmion is characterized by a non-zero integer topological charge Q given as an integral (18, 25, 26) of the topological density $q(x, y) = (1/4\pi) \mathbf{u} \cdot (\partial_x \mathbf{u} \times \partial_y \mathbf{u})$ over the xy plane perpendicular to the skyrmion string, where \mathbf{u} is a unit vector field defining the direction of the order parameter. In the case of the ferroelectric skyrmions the vector field \mathbf{u} is obtained from the local electric dipoles (17, 18). In particular, the PbTiO_3 skyrmion shown in Fig. 1a yields a topological charge of +1, common to Néel magnetic skyrmions in GaV_4S_8 (27) as well as Bloch magnetic skyrmions in MnSi (1, 4). In contrast, we report here a stable ferroelectric nanodomain carrying a topological charge of $Q = -2$.

Geometrical considerations

It can be guessed that nanodomains of antiparallel polarization in PbTiO_3 look roughly like in Fig. 1a and that of BaTiO_3 look as in Fig. 1b and 1c. In particular, it can be inferred from the electrostatics that the boundaries would tend to be parallel to the direction of the spontaneous ferroelectric polarization and that the overall shape will agree with the macroscopic crystal symmetry of the ferroelectric domain. To state it more precisely, we describe the crystallographic directions and planes with Muller indices of the parent cubic structure, and the subset of planes equivalent with respect to the given ferroelectric domain state symmetry are denoted by the brackets with an asterisk superscript ($\{\}^*$). Furthermore, we introduced two Cartesian systems, (x, y, z) and (x', y', z') , in order to refer to the usual orientation of the axes within the ground state of PbTiO_3 and BaTiO_3 , resp., see Fig. 1. We note that for the tetragonal ferroelectric PbTiO_3 , $x \parallel [100]$ and the unique ferroelectric axis is $z \parallel [001]$, while in the trigonal ferroelectric groundstate of BaTiO_3 , $x' \parallel [01-1]$ and the unique ferroelectric axis is set as $z' \parallel [111]$. Knowing that the reported stable skyrmionic nanodomains in PbTiO_3 are delimited by 180-degree domain walls with $\{100\}^*$ orientations (Fig. 1a), we speculated that stable nanodomains in BaTiO_3 are delimited either by $\{1-10\}^*$ facets or by $\{2-1-1\}^*$ facets, since

both are low-index planes parallel to the ferroelectric axis z' . Using the convention of Ref. (28), we can state that PbTiO_3 skyrmions are formed by the neutral $\text{T180}\{100\}$ domain walls, while the stable nanodomains in rhombohedral BaTiO_3 are expected to be delimited by either $\text{R180}\{1-10\}$ domain walls (as in Fig. 1b) or by the $\text{R180}\{2-1-1\}$ domain walls (as in Fig. 1c).

It is worth noting that a necessary requirement for nonzero Q is a non-coplanar order parameter texture. Clearly, the non-coplanarity of the polarization profile of the PbTiO_3 nanodomain in Fig. 1a is related to the anticipated non-collinear, Bloch-like (chiral) structure of its $\text{T180}\{100\}$ domain walls (29). Likewise, in BaTiO_3 , according to the phenomenological Ginzburg-Landau theory and DFT calculations, both $\text{R180}\{1-10\}$ and $\text{R180}\{2-1-1\}$ domain walls should have a strongly non-collinear character (28, 30, 31). In this respect, rhombohedral BaTiO_3 appears to be a natural candidate for searching interesting topological defects.

Results

Since the exact shape and respective energy of $\text{R180}\{1-10\}$ and $\text{R180}\{2-1-1\}$ domain walls of BaTiO_3 happens to be sensitive to the parametrization of the Ginzburg-Landau potential (31, 32), we have employed here an *ab initio*-based atomistic shell model potential developed for BaTiO_3 by Sepiarski and coworkers (33). Typically, we have used supercells made of $12 \times 12 \times 4$ hexagonal unit cells (*i.e.*, 8640 independent atoms) with periodic boundary conditions. Stable topological defects in the ferroelectric ground state were searched for through relaxing various initial configurations using classical molecular dynamics simulations at the temperature of 1 K.

In order to avoid any bias towards the nonzero topological charge, most of our initial configurations were collinear polarization textures. We have started with a homogeneously polarized supercell with $P_{z'} < 0$ and inverted polarization in a columnar region of hexagonal cross-section, corresponding to Fig. 1b. The inner diameter D of the hexagonal area of positive $P_{z'}$ is given by $D \approx N \cdot d$, where d is the nominal spacing of the (1-10) Ti planes in the parent cubic phase, and N is the dimensionless diameter of the hexagon.

The relaxed structure obtained from such a topologically trivial bubble nanodomain with $N = 11$, $D \approx 3$ nm, is shown in Fig. 2a. While the overall columnar shape persisted and the $P_{z'}$ components did not change much, a considerable in-plane polarization components developed spontaneously in the circumference of the nanodomain. The in-plane polarization, represented by the arrows in Fig. 2a, forms six different vortices, with alternatively clockwise and anticlockwise sense of polarization rotation, each centered at one of the edges of the hexagon. Fig. 2b shows the simplified sketch of the polarization arrangement obtained, emphasizing the interlinked components of the reversed out-of-plane and swirling in-plane polarization. Fig. 2c shows the topological density of this relaxed state, which presents six pronounced local minima in the center of each vortex and six rather small maxima near the vertices of the hexagon. Integrating this topological density, the total topological charge of $Q = -2$ was neatly obtained. Therefore, this topological defect deserves to be called ferroelectric antiskyrmion.

Stability

The relaxed configuration shown in Fig. 2 corresponds to the local energy minimum – its stability with respect to infinitesimal perturbations has been confirmed by checking the sign of all eigenvalues of the dynamical matrix corresponding to the internal lattice degrees of freedom of the supercell. In order to further appreciate the robustness of the antiskyrmion configuration, we have also attempted to erase the nanodomain by a strong electric field aligned along the z'

axis. It turned out that the nanodomain is stable in a very broad range of $-850 \text{ kV/cm} < E'_z < 1000 \text{ kV/cm}$. In this range, the topological charge is always equal to -2. Since the critical fields are only 4-5 times less than the ideal coercive field limit for the homogeneous switching of the single domain state ($E_c = 4600 \text{ kV/cm}$), we conclude that this ferroelectric antiskyrmion is a remarkably resistant object.

Uniqueness of the antiskyrmion state

We have noticed that the diameter of the antiskyrmion defining the width of the $P_{z'} > 0$ area is comparable with the smearing of the $P_{z'}(x')$ domain wall profiles (Fig. 2d). Therefore, we have attempted to stabilize antiskyrmons of different sizes by varying the size of the initial topologically trivial nanodomains (see Fig. 3). The smallest antiskyrmion that we could create had $N = 9$ (see Fig. 3b). For smaller initial diameters, the nanodomain decays back to the single domain ground state (see Fig. 3a). The $N = 13$ antiskyrmion is shown in Fig. 3. All solutions share the $Q = -2$ topological charge and similar geometry.

We have also explored stability of other initial nanodomain configurations. In general, we have observed that simple inversion of $P_{z'}$ within a compact columnar nanodomain with a diameter of 3-4nm typically trigger a natural evolution towards the $Q = -2$ state. In spite of certain structural variations, the persistent topological defects share the same overall geometry (see Fig. 4c, 4i, 4j and 2a). In particular, the final antiskyrmion texture does not depend on whether the initial nanodomain has R180{1-10} or R180{2-1-1} domain walls (compare Fig. 2a and 4a). In other cases, the initial nanodomains evolved to the single domain state. For instance, the configuration similar to Fig. 2a but with inverted in-plane polarization is not stable (see Fig. 4b). In overall, these results indicate that the antiskyrmion solution is much more stable than any other columnar nanodomain that we have tested.

Discussion

It is worth noting that magnetic antiskyrmonic defects with $Q < 0$ are known (34), and they can even be derived from the canonical Bogdanov-Yablonskii phenomenological theory (35, 36). Nevertheless, the parent paraelectric phase of BaTiO₃ is centrosymmetric, so that the formal ferroelectric analogue (37) of the bulk Dzialoshinskii-Moriya interaction is forbidden. Therefore, the Bogdanov-Yablonskii theory (35) does not explain the existence of the antiskyrmons investigated in this work, and we can also exclude the interfacial Dzialoshinskii-Moriya mechanism (38) since there is no interface in our simulations.

Likewise, the bulk skyrmion stabilization scenario of PbTiO₃, based on the emergence of Bloch character of the domain walls, does not apply to the formation of antiskyrmons in the rhombohedral ferroelectric phase of BaTiO₃. In fact, borders of BaTiO₃ antiskyrmion do not have Bloch-like character. Indeed, the transverse polarization component $P_{y'}$ at the wall of the BaTiO₃ antiskyrmion is changing its sign, unlike in the Bloch wall (see Fig. 2d). Such domain walls, called bichiral walls (39, 40), have been previously considered to exist in BaTiO₃ (28, 30), but their existence does not immediately imply the stability of the antiskyrmion.

While we are not aware of any investigations of a similar ferroelectric antiskyrmion defects, the higher-skyrmion number $|Q| > 1$ have been already considered for magnetic systems (41–44). The geometrically closest textures described in the literature are probably the $Q = -2$ motifs in the magnetic textures of triangular magnets (41, 42) and ultrathin magnetic films (45, 46). Although the magnetic interactions are very different from the ferroelectric ones, phases of triangular magnets may serve as an inspiration for investigations of the condensation of the

isolated ferroelectric antiskyrmions into the ferroelectric antiskyrmionic lattices. One of the remarkable common aspect of these magnetic and ferroelectric antiskyrmions is that the topological density is concentrated only to a few “hot spots” with fractional topological charge (18, 42, 47). In the present ferroelectric antiskyrmion, there are six such hot spots, each carrying a “quark-like” topological charge of $Q \approx -1/3$.

Conclusion

In summary, we studied extremely small columnar ferroelectric nanodomains in the low-temperature ferroelectric phase of BaTiO₃ by means of established ab-initio based atomistic methodology (33, 48-50).

We realized not only that the ferroelectric nanodomains with a miniscule 2-4nm diameter can be stabilized, but also that these nanodomains have a characteristic hexagonal shape and that six vortices develop, each on one facet of the nanodomain, and each carrying a fractional topological charge of about -1/3, giving altogether the unusual net skyrmion number of -2. We computationally affirmed the stability of these ferroelectric antiskyrmions, their remarkable resilience to the electric fields and temperature fluctuations, and explored the kinetics of their formation.

This work indicates that nanoscale ferroelectric topological defects exists not only in PbTiO₃, but also in other ferroelectric materials, and that distinct ferroelectric materials can carry completely different kinds of truly nanoscale topological defects. We believe that these findings will propel further experimental and theoretical developments of ferroelectric skyrmionics.

Methods

Interatomic potential. For all atomistic calculations/simulations in this study we used the interatomic potential by Sepiarsky et al. (33), which has been parametrized on the basis of an ab-initio-derived set of BaTiO₃ attributes. The potential utilizes the framework of the shell model, which by representing each atom with a core and a shell mimics atomic polarizability, and with the anharmonic core-shell interaction is particularly well-suited to reproducing ferroelectric behaviour (48). In particular, the parametrization predicts correct sequence of BaTiO₃ phase transitions (with the $T_C \approx 360$ K and the rhombohedral phase explored here stable below ~ 140 K (48)).

Nanodomain construction and relaxation. We worked with supercells made of $12 \times 12 \times 4$ rhombohedral BaTiO₃ unit cells in the hexagonal setting (*i.e.* 8640 atoms) subjected to periodic boundary conditions. The initial polarization configurations were set by displacing the Ti atoms from the centres of oxygen octahedra along the z' direction (positive displacement in the nanodomain and negative in the matrix). The Ti atoms in the one-atom-thick layer at the domain boundary remained in the ideal cubic positions.

Classical molecular dynamics (MD) simulations were taken as the main engine for structure relaxation of the studied systems. To this end the DL POLY software (49) was used and the calculations were done with constant strain – constant temperature ensemble, 0.4 ps timestep and 10 ps initial equilibration time. Temperature was set to 1 K to allow the structures for effective relaxation involving small amount of thermal noise. The systems were kept evolving for several tens of ps, until no change in the time-averaged local dipole configurations could be observed (usually after ~ 10 ps of the production run).

To confirm that the obtained relaxed configurations are in energetic minima, the atomic positions were subjected to rational function optimization method as implemented in the program GULP (50). The method consists in diagonalization of the Hessian and it follows the modes with the smallest eigenvalues in the optimization process. We found that the MD-derived structures needed no meaningful steps in the optimization with the minuscule reduction of the energy (<0.1 eV per 5-atom formula unit). Final check of stability comprised calculation of a dynamical matrix and its eigenvalues (also within GULP) to exclude any remnant unstable modes.

Local dipole moments of structures chosen for the presentation were evaluated for each 5-atom perovskite cell separately on the basis of positions and charges of cores and shells. For a given cell one Ti atom with its surrounding octahedron of six O atoms (with the weight 0.5) and 8 coordinating Ba atoms (0.125 weight) was considered.

References and notes:

1. S. Mühlbauer, B. Binz, F. Jonietz, C. Pfleiderer, A. Rosch, A. Neubauer, R. Georgii, P. Böni, Skyrmion lattice in a chiral magnet. *Science* **323**, 915–919 (2009). doi: 10.1126/science.1166767
2. U. K. Rößler, A. N. Bogdanov, C. Pfleiderer, Spontaneous skyrmion ground states in magnetic metals. *Nature* **442**, 797–801 (2006). doi: 10.1038/nature05056
3. A. Fert, N. Reyren, V. Cros, Magnetic skyrmions: advances in physics and potential applications. *Nat. Rev. Mater.* **2**, 17031 (2017). doi: 10.1038/natrevmats.2017.31
4. A. Neubauer, C. Pfleiderer, B. Binz, A. Rosch, R. Ritz, P. G. Niklowitz, P. Böni, Topological Hall effect in the A phase of MnSi. *Phys. Rev. Lett.* **102**, 186602 (2009). doi: 10.1103/PhysRevLett.102.186602
5. T. Schulz, R. Ritz, A. Bauer, M. Halder, M. Wagner, C. Franz, C. Pfleiderer, K. Everschor, M. Garst, A. Rosch, Emergent electrodynamics of skyrmions in a chiral magnet. *Nat. Phys.* **8**, 301–304 (2012). doi: 10.1038/nphys2231
6. P. Bruno, V. K. Dugaev, M. Taillefumier, Topological Hall effect and Berry phase in magnetic nanostructures. *Phys. Rev. Lett.* **93**, 096806 (2004). doi: 10.1103/PhysRevLett.93.096806
7. J. Zang, M. Mostovoy, J. H. Han, N. Nagaosa, Dynamics of skyrmion crystals in metallic thin films. *Phys. Rev. Lett.* **107**, 136804 (2011). doi: 10.1103/PhysRevLett.107.136804
8. K. Litzius, I. Lemesh, B. Krüger, P. Bassirian, L. Caretta, K. Richter, F. Büttner, K. Sato, O. A. Tretiakov, J. Förster, R. M. Reeve, M. Weigand, I. Bykova, H. Stoll, G. Schütz, G. S. D. Beach, M. Kläui, Skyrmion Hall effect revealed by direct time-resolved X-ray microscopy. *Nat. Phys.* **13**, 170–175 (2017). doi: 10.1038/nphys4000
9. W. Jiang, X. Zhang, G. Yu, W. Zhang, X. Wang, M. B. Jungfleisch, J. E. Pearson, X. Cheng, O. Heinonen, K. L. Wang, Y. Zhou, A. Hoffmann, S. G. E. te Velthuis, Direct observation of the skyrmion Hall effect. *Nat. Phys.* **13**, 162–169 (2017). doi: 10.1038/nphys3883
10. Y. Fujishiro, N. Kanazawa, T. Nakajima, X. Z. Yu, K. Ohishi, Y. Kawamura, K. Kakurai, T. Arima, H. Mitamura, A. Miyake, K. Akiba, M. Tokunaga, A. Matsuo, K. Kindo, T.

Koretsune, R. Arita, Y. Tokura, Topological transitions among skyrmion-and hedgehoglattice states in cubic chiral magnets. *Nat. Commun.* **10**, 1059 (2019). doi: 10.1038/s41467-019-08985-6

11. N. Kent, N. Reynolds, D. Raftrey, I. T. G. Campbell, S. Virasawmy, S. Dhuey, R. V. Chopdekar, A. Hierro-Rodriguez, A. Sorrentino, E. Pereiro, S. Ferrer, F. Hellman, P. Sutcliffe, P. Fischer, Creation and observation of Hopfions in magnetic multilayer systems. *Nat. Commun.* **12** 1562 (2021). doi: 10.1038/s41467-021-21846-5

12. S. Zhang, F. Kronast, G. van der Laan, T. Hesjedal, Real-space observation of skyrmionium in a ferromagnetmagnetic topological insulator heterostructure. *Nano Lett.* **18**, 1057–1063 (2018). doi: 10.1021/acs.nanolett.7b04537

13. M. Finazzi, M. Savoini, A. R. Khorsand, A. Tsukamoto, A. Itoh, L. Duò, A. Kirilyuk, Th. Rasing, M. Ezawa, Laser-induced magnetic nanostructures with tunable topological properties. *Phys. Rev. Lett.* **110**, 177205 (2013). doi: 10.1103/PhysRevLett.110.177205

14. J. Barker, O. A. Tretiakov, Static and dynamical properties of antiferromagnetic skyrmions in the presence of applied current and temperature. *Phys. Rev. Lett.* **116**, 147203 (2016). doi: 10.1103/PhysRevLett.116.147203

15. C. Back, V. Cros, H. Ebert, K. Everschor-Sitte, A. Fert, M. Garst, Tianping Ma, S. Mankovsky, T. L. Monchesky, M. Mostovoy, N. Nagaosa, S. S. P. Parkin, C. Pfleiderer, N. Reyren, A. Rosch, Y. Taguchi, Y. Tokura, K. von Bergmann, Jiadong Zang, The 2020 skyrmionics roadmap. *J. Phys. D: Appl. Phys.* **53**, 363001 (2020). doi: 10.1088/1361-6463/ab8418

16. S. Das, Y. L. Tang, Z. Hong, M. A. P. Gonçalves, M. R. McCarter, C. Klewe, K. X. Nguyen, F. Gómez-Ortiz, P. Shafer, E. Arenholz, V. A. Stoica, S.-L. Hsu, B. Wang, C. Ophus, J. F. Liu, C. T. Nelson, S. Saremi, B. Prasad, A. B. Mei, D. G. Schlom, J. Íñiguez, P. García-Fernández, D. A. Muller, L. Q. Chen, J. Junquera, L. W. Martin & R. Ramesh, Observation of room-temperature polar skyrmions. *Nature* **568**, 368–372 (2019). doi: 10.1038/s41586-019-1092-8

17. M. A. P. Gonçalves, C. Escorihuela-Sayalero, P. García-Fernández, J. Junquera, J. Íñiguez, Theoretical guidelines to create and tune electric skyrmion bubbles. *Science Advances* **5**, eaau7023 (2019). doi: 10.1126/sciadv.aau7023

18. Y. Nahas, S. Prokhorenko, L. Louis, Z. Gui, I. Kornev, L. Bellaiche, Discovery of stable skyrmionic state in ferroelectric nanocomposites. *Nat. Commun.* **6**, 8542 (2015). doi: 10.1038/ncomms9542

19. S. Das, Z. Hong, V. A. Stoica, M. A. P. Gonçalves, Y. T. Shao, E. Parsonnet, E. J. Marksz, S. Saremi, M. R. McCarter, A. Reynoso, C. J. Long, A. M. Hagerstrom, D. Meyers, V. Ravi, B. Prasad, H. Zhou, Z. Zhang, H. Wen, F. Gómez-Ortiz, P. García-Fernández, J. Bokor, J. Íñiguez, J. W. Freeland, N. D. Orloff, J. Junquera, L. Q. Chen, S. Salahuddin, D. A. Muller, L. W. Martin, R. Ramesh, Local negative permittivity and topological phase transition in polar skyrmions. *Nat. Mater.* **20**, 194–201 (2021). doi: 10.1038/s41563-020-00818-y

20. R. Zhu, Z. Jiang, X. Zhang, X. Zhong, C. Tan, M. Liu, Y. Sun, X. Li, R. Qi, K. Qu, Z. Liu, M. Wu, M. Li, B. Huang, Z. Xu, J. Wang, K. Liu, P. Gao, J. Wang, J. Li, X. Bai, Dynamics of polar skyrmion bubbles under electric fields. *Phys. Rev. Lett.* **129**, 107601 (2022). doi: 10.1103/PhysRevLett.129.107601

21. K. T. Kim, M. R. McCarter, V. A. Stoica, S. Das, C. Klewe, E. P. Donoway, D. M. Burn, P. Shafer, F. Rodolakis, M. A. P. Gonçalves, F. Gómez-Ortiz, J. Íñiguez, P. García-Fernández, J. Junquera, S. Susarla, S. W. Lovesey, G. van der Laan, S. Y. Park, L. W. Martin, J. W. Freeland, R. Ramesh, D. R. Lee, Chiral structures of electric polarization vectors quantified by x-ray resonant scattering. *Nat. Commun.* **13**, 1769 (2022). doi: 10.1038/s41467-022-29359-5
22. Yu. Tikhonov, S. Kondovych, J. Mangeri, M. Pavlenko, L. Baudry, A. Sené, A. Galda, S. Nakhmanson, O. Heinonen, A. Razumnaya, I. Luk'yanchuk, V. M. Vinokur, Controllable skyrmion chirality in ferroelectrics. *Sci. Rep.* **10**, 8657 (2020). doi: 10.1038/s41598-020-65291-8
23. P. Shafer, P. García-Fernández, P. Aguado-Puente, A. R. Damodaran, A. K. Yadav, C. T. Nelson, S.-L. Hsu, J. C. Wojdeł, J. Íñiguez, L. W. Martin, E. Arenholz, J. Junquera, R. Ramesh, Emergent chirality in the electric polarization texture of titanate superlattices. *Proceedings of the National Academy of Sciences* **115**, 915–920 (2018). doi: 10.1073/pnas.1711652115
24. Y.-T. Shao, S. Das, Z. Hong, R. Xu, S. Chandrika, F. Gómez-Ortiz, P. García-Fernández, L.-Q. Chen, H. Y. Hwang, J. Junquera, L. W. Martin, R. Ramesh, D. A. Muller, Emergent chirality in a polar meron to skyrmion phase transition. <https://arxiv.org/abs/2101.04545> (2021).
25. S. Seki, M. Mochizuki, *Skyrmions in Magnetic Materials* (Springer International Publishing, 2016).
26. N. Nagaosa, Y. Tokura, Topological properties and dynamics of magnetic skyrmions. *Nat. Nanotech.* **8**, 8579–8589 (2013). doi: 10.1038/nnano.2013.243
27. I. Kézsmárki, S. Bordács, P. Milde, E. Neuber, L. M. Eng, J. S. White, H. M. Rønnow, C. D. Dewhurst, M. Mochizuki, K. Yanai, H. Nakamura, D. Ehlers, V. Tsurkan, A. Loidl, Néel-type skyrmion lattice with confined orientation in the polar magnetic semiconductor GaV₄S₈. *Nat. Mater.* **14**, 1116–1122 (2015). doi: 10.1038/nmat4402
28. P. Marton, I. Rychetsky, and J. Hlinka, Domain walls of ferroelectric BaTiO₃ within the Ginzburg-Landau-Devonshire phenomenological model. *Phys. Rev. B* **81**, 144125 (2010). doi: 10.1103/PhysRevB.81.144125
29. J. C. Wojdeł and J. Íñiguez, Ferroelectric transitions at ferroelectric domain walls found from first principles. *Phys. Rev. Lett.* **112**, 247603 (2014). doi: 10.1103/PhysRevLett.112.247603
30. M. Taherinejad, D. Vanderbilt, P. Marton, V. Stepkova, J. Hlinka, Bloch-type domain walls in rhombohedral BaTiO₃. *Phys. Rev. B* **86**, 155138 (2012). doi: 10.1103/PhysRevB.86.155138
31. V. Stepkova, P. Marton, J. Hlinka, Stress-induced phase transition in ferroelectric domain walls of BaTiO₃. *J. Phys. Condens. Matter* **24**, 212201 (2012). doi: 10.1088/0953-8984/24/21/212201
32. J. Hlinka, V. Stepkova, P. Marton, P. Ondrejko, in *Topological Structures in Ferroic Materials*, J. Seidel, Ed. (Springer, Switzerland, 2016), pp. 161–180.
33. M. Sepliarsky, A. Asthagiri, S. R. Phillpot, M. G. Stachiotti, R. L. Migoni, Atomic-level simulation of ferroelectricity in oxide materials. *Curr. Opin. Solid State Mater. Sci.* **9**, 107–113 (2005). doi: 10.1016/j.cossms.2006.05.002

34. A. K. Nayak, V. Kumar, T. Ma, P. Werner, E. Pippel, R. Sahoo, F. Damay, U. K. Röbler, C. Felser, S. S. P. Parkin, Magnetic antiskyrmions above room temperature in tetragonal Heusler materials. *Nature* **548**, 561–566 (2017). doi: 10.1038/nature23466
35. A. N. Bogdanov, D. A. Yabloskii, Thermodynamically stable “vortices” in magnetically ordered crystals. The mixed state of magnets. *Zh. Eksp. Teor. Fiz.* **95**, 178–182 (1989).
36. A. N. Bogdanov, C. Panagopoulos, Physical foundations and basic properties of magnetic skyrmions. *Nat. Rev. Phys.* **2**, 492–498 (2020). doi: 10.1038/s42254-020-0203-7
37. K. C. Erb, J. Hlinka, Vector, bidirector, and Bloch skyrmion phases induced by structural crystallographic symmetry breaking. *Phys. Rev. B* **102**, 024110 (2020). doi: 10.1103/PhysRevB.102.024110
38. M. Hoffmann, B. Zimmermann, G. P. Müller, D. Schürhoff, N. S. Kiselev, C. Melcher, S. Blügel, Antiskyrmions stabilized at interfaces by anisotropic Dzyaloshinskii-Moriya interactions. *Nat. Commun.* **8**, 1–9 (2017). doi: 10.1038/s41467-017-00313-0
39. B. Houchmandzadeh, J. Lajzerowicz, E. Salje, Order parameter coupling and chirality of domain walls. *J. Phys. Condens. Matter* **3**, 5163 (1991). doi: 10.1088/0953-8984/3/27/009
40. P. V. Yudin, A. K. Tagantsev, E. A. Eliseev, A. N. Morozovska, and N. Setter, Bichiral structure of ferroelectric domain walls driven by flexoelectricity. *Phys. Rev. B* **86**, 134102 (2012). doi: 10.1103/PhysRevB.86.134102
41. N. Mohanta, E. Dagotto. Interfacial phase frustration stabilizes unconventional skyrmion crystals. *npj Quantum Mater.* **7**, 76 (2022). doi: 10.1038/s41535-022-00483-1
42. D. Amoroso, P. Barone, S. Picozzi, Spontaneous skyrmionic lattice from anisotropic symmetric exchange in a Ni-halide monolayer. *Nat. Commun.* **11**, 5784 (2020). doi: 10.1038/s41467-020-19535-w
43. R. Ozawa, S. Hayami, Y. Motome, Zero-field skyrmions with a high topological number in itinerant magnets. *Phys. Rev. Lett.* **118**, 147205 (2017). doi: 10.1103/PhysRevLett.118.147205
44. A. O. Leonov, M. Mostovoy, Multiply periodic states and isolated skyrmions in an anisotropic frustrated magnet. *Nat. Commun.* **6**, 8275 (2015). doi: 10.1038/ncomms9275
45. B. Dupé, C. N. Kruse, T. Dornheim, S. Heinze, How to reveal metastable skyrmionic spin structures by spin-polarized scanning tunneling microscopy. *New J. Phys.* **18**, 055015 (2016). doi: 10.1088/1367-2630/18/5/055015
46. S. Heinze, K. von Bergmann, M. Menzel, J. Brede, A. Kubetzka, R. Wiesendanger, G. Bihlmayer, S. Blügel, Spontaneous atomic-scale magnetic skyrmion lattice in two dimensions. *Nat. Phys.* **7**, 713–718 (2011). doi: 10.1038/nphys2045
47. S. Z. Lin, A. Saxena, C. D. Batista, Skyrmion fractionalization and merons in chiral magnets with easy-plane anisotropy. *Phys. Rev. B* **91**, 224407 (2015). doi: 10.1103/PhysRevB.91.224407
48. S. Tinte, M. G. Stachiotti, S. R. Phillpot, M. Sepiarsky, D. Wolf, R. L. Migoni, Ferroelectric properties of $\text{Ba}_x\text{Sr}_{1-x}\text{TiO}_3$ solid solutions obtained by molecular dynamics simulation. *J. Phys. Condens. Matter* **16**, 3495 (2004). doi: 10.1088/0953-8984/16/20/019
49. I. T. Todorov, W. Smith, K. Trachenko, M. T. Dove, DL POLY 3: new dimensions in molecular dynamics simulations via massive parallelism. *J. Mater. Chem.* **16**, 1911–1918 (2006). doi: 10.1039/b517931a

50. J. D. Gale, A. L. Rohl, The General Utility Lattice Program (GULP). *Mol. Simul.* **29**, 291–341 (2003). doi: 10.1080/0892702031000104887

Acknowledgments:

Funding:

This work was supported by the Czech Science Foundation (project no. 19-28594X).

Author contributions:

JH proposed the scope of the investigations and the outline of the paper; MAPG performed the ensemble of simulations under the guidance of MP; all authors discussed the intermediate progress and all equally contributed to the final manuscript.

Competing interests:

Authors declare that they have no competing interests.

Data and materials availability:

All data are available in the main text or upon a reasonable request from authors

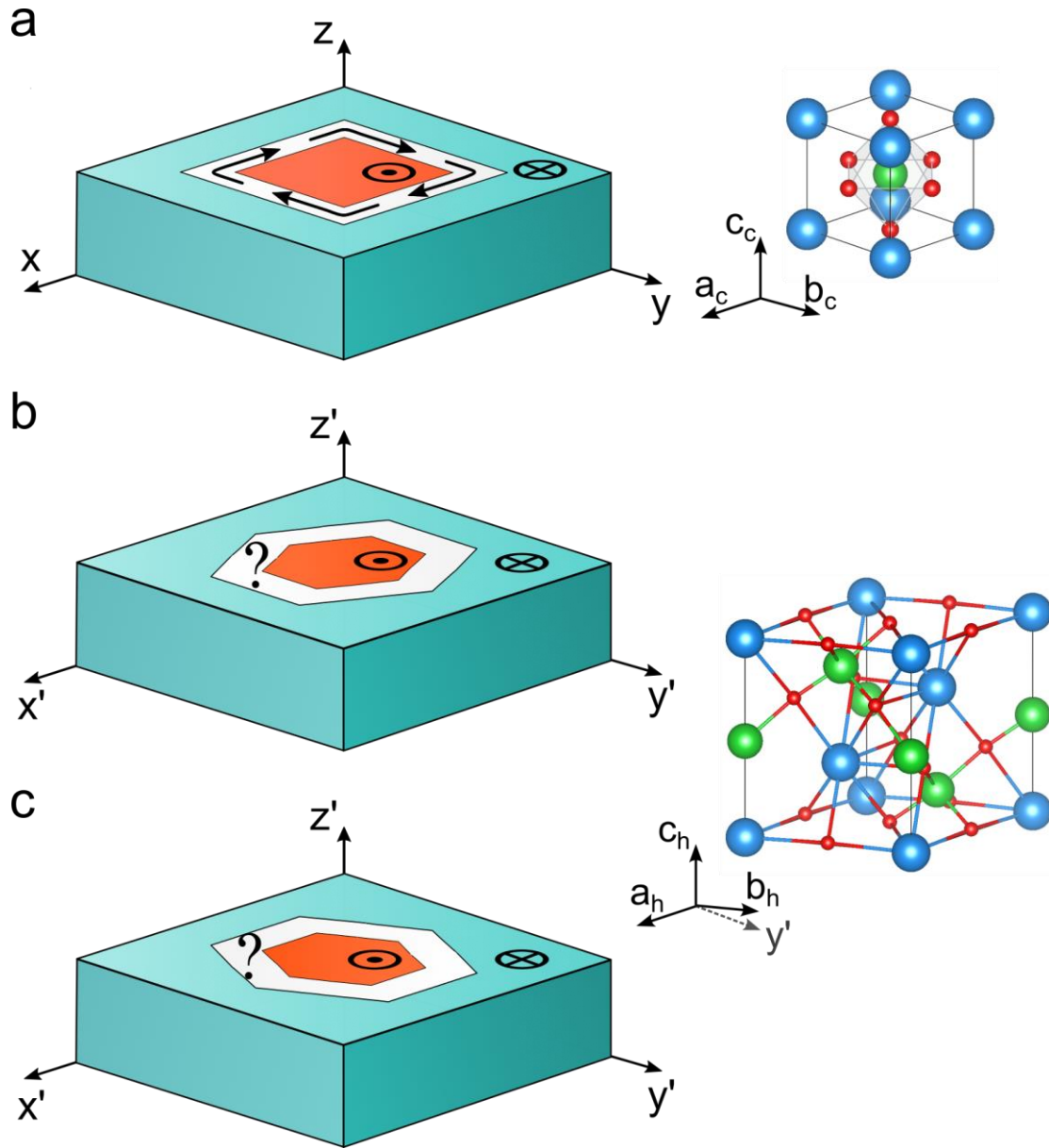


Fig. 1. Ultrasmall domains of antiparallel polarization in PbTiO_3 and BaTiO_3 . (a) Typical nanodomain configuration in tetragonal PbTiO_3 as identified in previous investigations (17). The polarization of the inner part (orange) is parallel to the ferroelectric z axis, the outer one (turquoise) has the opposite polarization. Black arrows in the domain wall region (white) represent the inner domain wall polarization forming a close loop around the nanodomain. (b) The anticipated shape of nanodomain within a rhombohedral BaTiO_3 with the ferroelectric axis $z' \parallel [111]$. Domain walls are parallel to the $\{1-10\}^*$ crystallographic planes. (c) Similar configuration but with domain walls parallel to the $\{-211\}^*$ crystallographic planes. On the top right side, the respective orientation of the parent cubic perovskite unit cell is plot along with the lattice vectors a_c , b_c and c_c , while on the bottom right, the same structure is redrawn within the hexagonal cell adapted to the symmetry of rhombohedral BaTiO_3 ($a_h = (0, 1, -1)$ and $b_h = (-1, 0, 1)$ are not orthogonal). The blue spheres stand for the Pb or Ba atoms, the green ones are the Ti atoms, and the red ones are the O atoms.

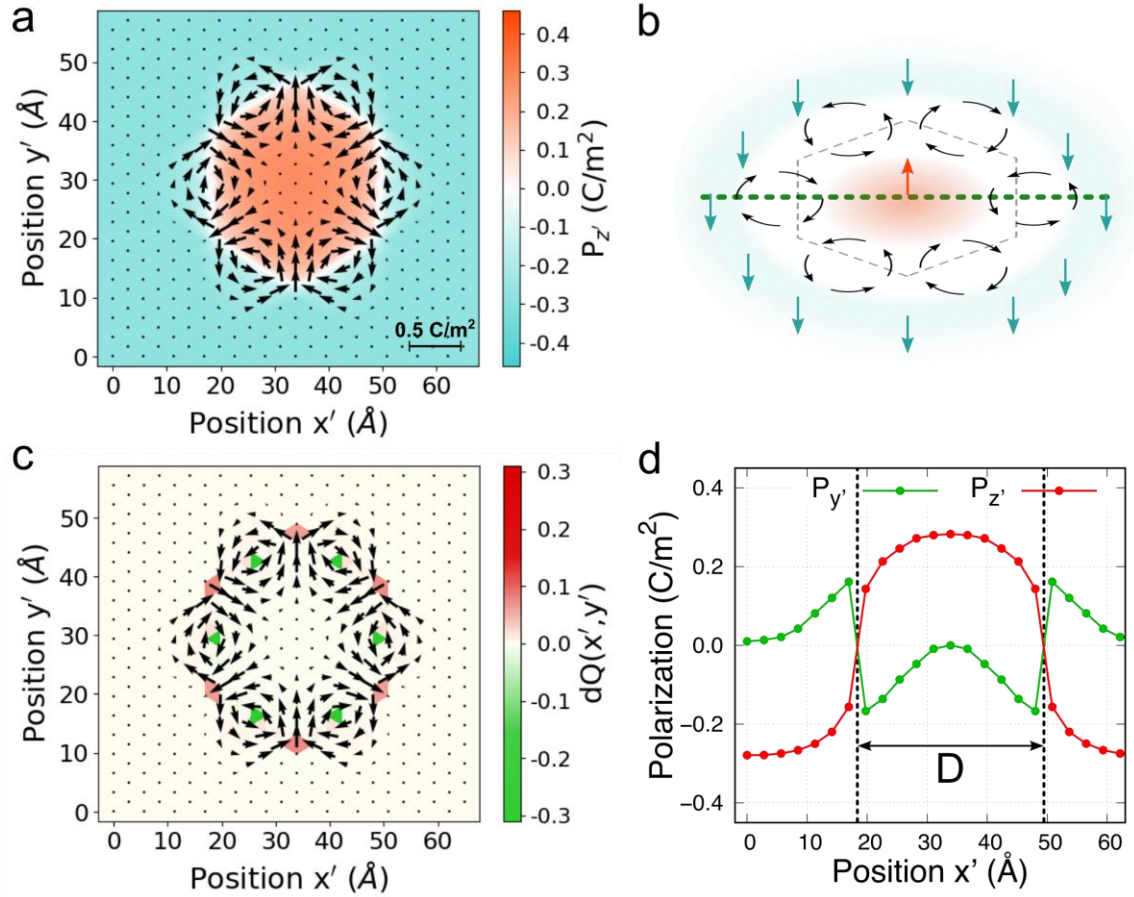


Fig. 2. A relaxed antiskyrmion nanodomain in rhombohedral BaTiO₃. (a) Section through the $N = 11$ antiskyrmion polarization configuration obtained by relaxation of a topologically trivial bubble nanodomain with the hexagonal geometry of Fig. 1b. Local polarization is calculated for each Ti site and projected along the z' axis. Non-negligible in-plane polarization components are marked by arrows, the out of plane components are indicated by color. (b) Simplified sketch of the same polarization pattern. The orange and turquoise arrows represent the nanodomain and the matrix. Curved arrows are indicating the six vortices of in-plane polarization part. (c) Topological charge density distribution $q(x', y')dS$ superposed with the in-plane polarization. Values of $q(x', y')dS$ are calculated separately for each individual triangular plaquette within the triangular sublattice of the projected Ti positions. (d) Transversal polarization components $P_{x'}$, $P_{z'}$ along the green dashed line of panel (b) with indicated skyrmion size D .

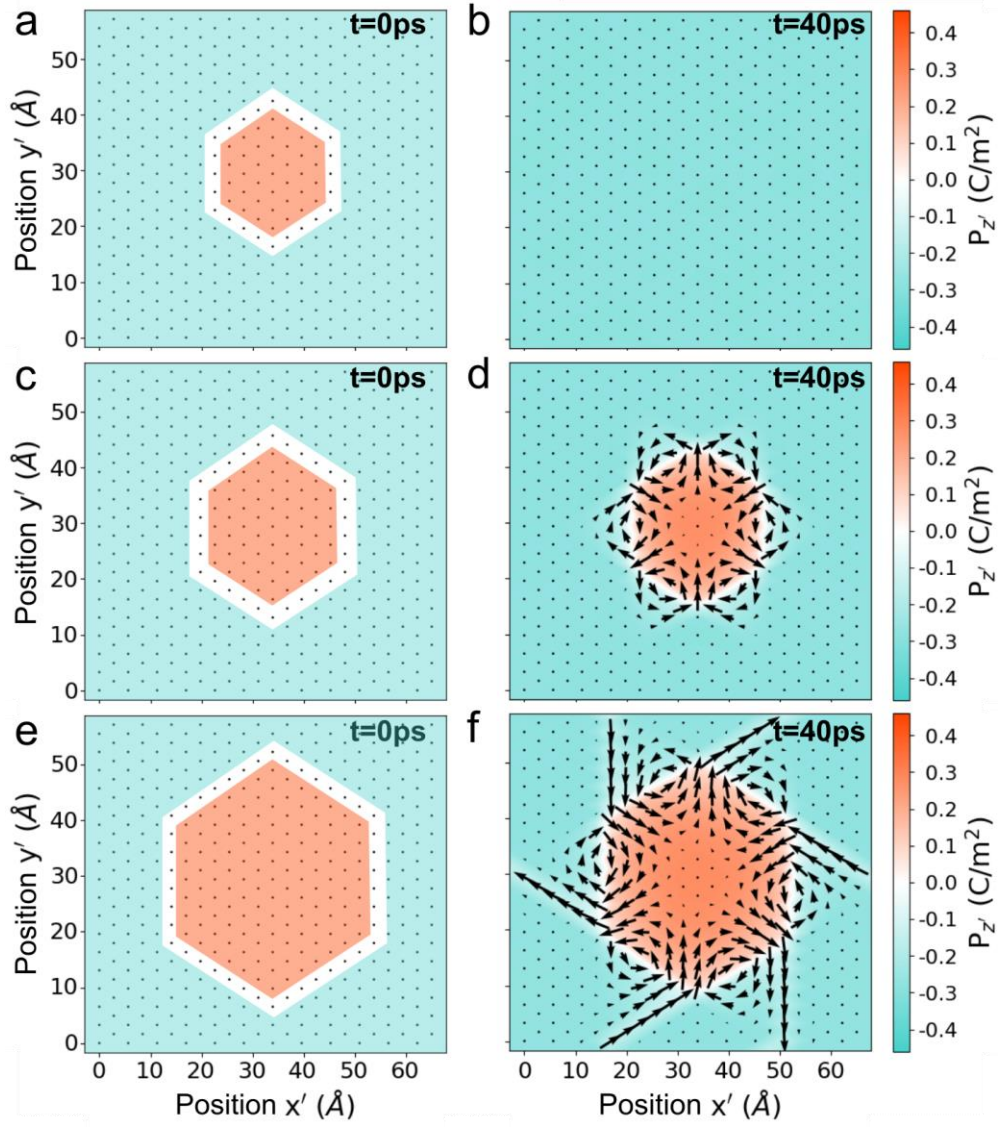


Fig. 3. Formation of antiskyrmions with different sizes. Left panels (a, c, e) show the initial nanodomain with a topologically trivial colinear polarization configuration. From top to bottom, the size parameter is $N = 7$, $N = 9$ and $N = 13$. Right panels (b, d, f) show the respective relaxed configuration after 40 ps of MD relaxation at $T = 1$ K.

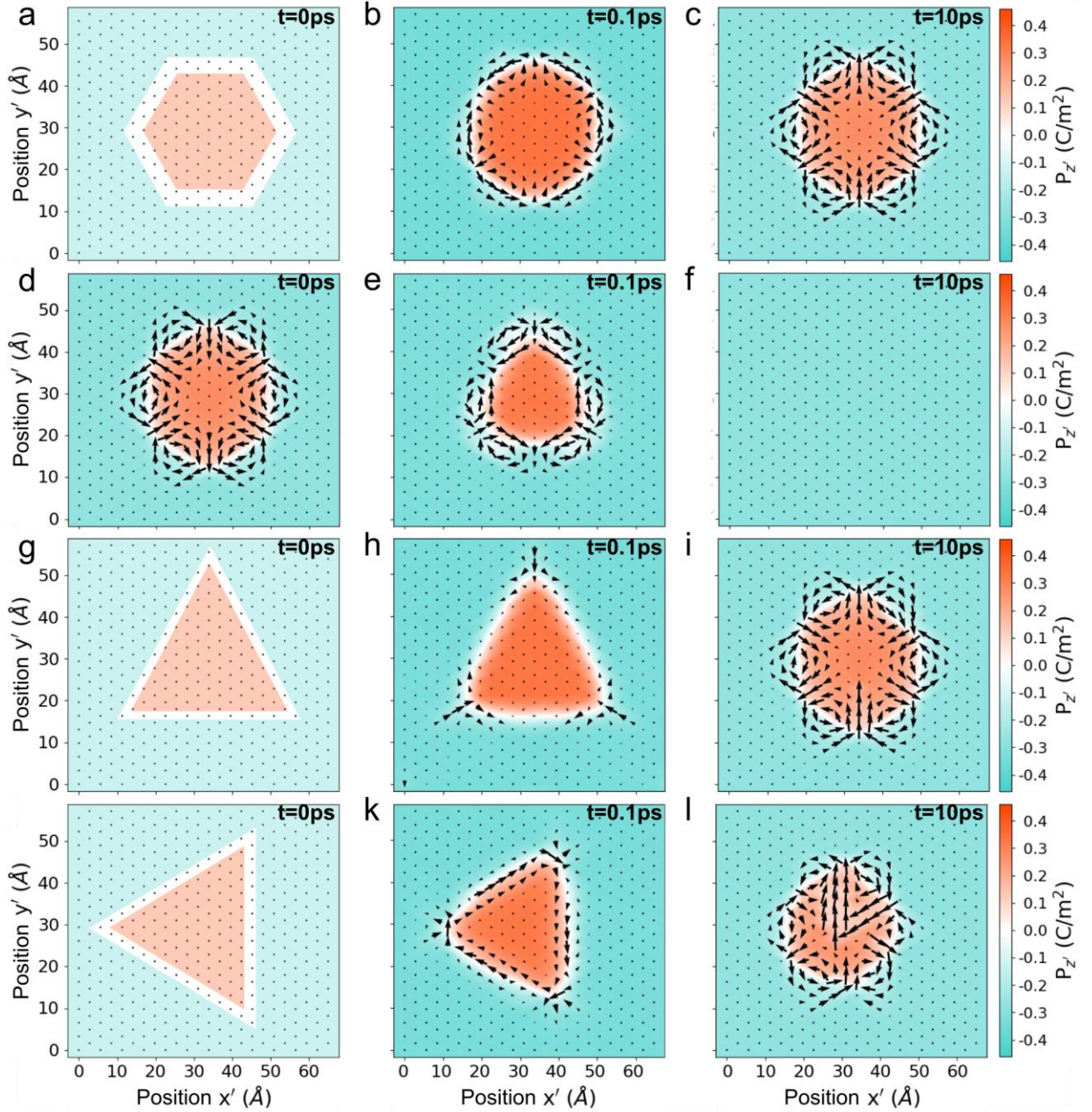


Fig. 4. Decay of alternative initial configurations. Left panels show the initial configurations, middle panels show the structures after 0.1 ps of MD evolution and the right panels show the close to final equilibrium configuration registered after 10 ps of MD evolution. (a, b, c) – configuration R180{-211} domain walls transform to that with R180{01-1} domain walls. (d, e, f) – configuration similar to Fig. 2a but with inverted in-plane polarization decays into the single domain. (g, h, i) and (j, k, l) – evolution from the low-symmetry colinear configurations with R180{-211} and R180{01-1} domain walls, respectively.